Catalysis Letters, Vol. 116, Nos. 1–2, July 2007 (© 2007)
DOI: 10.1007/s10562-007-9124-7

Effect of alloy composition on dispersion stability and catalytic activity for NO oxidation over alumina-supported Pt–Pd catalysts

G. W. Graham,[a] H.-W. Jen,[a] O. Ezekoye,[b] R. J. Kudla,[a] W. Chun,[a] X. Q. Pan,[b] and R. W. McCabe[a,*]

[a]*Chemical Engineering Department, Ford Motor Company, 2101 Village Road, MD3179/RIC, Dearborn, MI 48121-2053, USA*
[b]*Department of Material Science & Engineering, University of Michigan, 2300 Hayward Street, Ann Arbor, MI 48109-2136, USA*

Received 20 March 2007; accepted 11 April 2007

Applying a synthesis procedure that promotes alloy formation, highly-dispersed alumina-supported Pt–Pd catalysts spanning the Pt-rich half of the composition range were prepared, aged under oxygen-rich hydrothermal conditions, and characterized by CO chemisorption, XRD, and TEM. Anomalously large particles, typical of pure Pt catalysts treated under such conditions, were not found in any of the Pd-containing catalysts, and the extent of particle coarsening due to aging was found to decrease with increasing Pd content. Alloying appears to have little effect on the NO oxidation turn-over frequency, which increases with decreasing dispersion.

KEY WORDS: Pt; Pd; alloy; particle coarsening; NO oxidation.

1. Introduction

Oxidation of NO plays a prominent role in the catalytic after-treatment of exhaust gas from lean-combustion vehicles. It is an important step in the overall reaction that leads to NO storage in the NO_x-storage/reduction (NSR) catalyst [1]. It is also desirable for improving low-temperature efficiency of the NO selective catalytic reduction (SCR) catalyst, based on NH_3 [2], and critical to the operation of the continuously regenerating diesel particulate (soot) filter [3].

Pt is generally regarded as one of the best catalysts for NO oxidation, but supported Pt catalysts tend to lose Pt surface area rapidly under high-temperature lean conditions due to Pt-particle coarsening [4]. Alloying Pt with metals such as Pd or Rh has been proposed as a possible means of retarding such coarsening [5], but few systematic studies of alloying on the dispersion stability of supported catalysts have been performed [6]. Further, the effect of alloying on NO oxidation activity has not been determined over a wide range of dispersions [7]. In this study, we prepared a series of highly-dispersed Pt–Pd catalysts, and aged, characterized, and tested them with the specific intent of assessing these effects. The aging experiments were carried out in the laboratory at various temperatures, but with a fixed time and in simplified exhaust gas compositions. We show that alloying Pt with Pd in alumina-supported catalysts (up to ~50 mol%), stabilizes the metal particle size within a near-optimal range after aging without adversely affecting the turn-over frequency compared to pure Pt. From a practical point of view, these results suggest that Pt can be partially substituted with less expensive Pd while improving catalyst durability and without significantly sacrificing NO oxidation performance. Further evaluation is needed, however, to examine the effect of aging time, as well as to confirm the benefits under actual in-use conditions.

*To whom correspondence should be addressed.
E-mail: rmccabe@ford.com

2. Experimental details

2.1. Catalyst preparation

Catalysts were prepared by adsorption from solutions of mixtures of platinum(II) and palladium(II) bis-acetylacetonates in toluene at 70 °C onto a high-surface-area alumina (W. R. Grace, MI-307), a procedure that reportedly favors the formation of bimetallic particles over a wide range of compositions [8,9]. The extent of adsorption, determined through uv–vis spectrophotometry of the solutions, provided the means for estimation of the catalyst compositions listed in table 1. (The target loading was a constant, combined-metal *molar* level corresponding to that of 1wt% Pt, but adsorption of the pure Pt salt was limited, allowing a maximum obtainable loading of only 0.87wt% Pt. Absorption of the pure Pd salt, on the other hand, was very efficient. The column labeled "Equivalent Pt (wt%)" in table 1 thus provides an indication of the degree to which the target was met.) After drying at 70 °C under vacuum, catalysts were calcined at 300 °C in 5% O_2 in N_2 and reduced in 1% H_2 in N_2 at 300 °C.

Table 1
Catalysts

Catalyst name	Composition (wt%)		Atom fraction		Equivalent Pt (wt%)
	(Pt)	(Pd)	(Pt)	(Pd)	
Pt-100-Pd-0	0.87	0	100	0	0.87
Pt-90-Pd-10	0.75	0.063	87	13	0.87
Pt-80-Pd-20	0.70	0.11	78	22	0.90
Pt-50-Pd-50	0.58	0.28	53	47	1.09
Pt-0-Pd-100	0	0.56	0	100	1.03

2.2. Catalyst aging

Catalyst samples were aged in a quartz-tube furnace under a flowing (5 l/min) gas mixture of 5% O_2 and 10% H_2O in N_2. Aging temperatures were 500, 600, 750, and 900 °C, and time spent at each was 3 h. (Heating and cooling occurred under pure N_2.) Subsequently, the samples were reduced for 1 h at 500 °C under a flow of 1% H_2 in N_2. The specific surface area of Pt-100-Pd-0 was 157 m^2/g after aging at 500 °C and 134 m^2/g after aging at 900 °C.

2.3. CO chemisorption

2.3.1. CO adsorption capacity

CO adsorption capacity was measured by the volumetric method using a system made by Advanced Scientific Design, Inc. Approximately 200 mg of catalyst sample was pretreated in a flow (50 ml/min) of 5% H_2 in N_2 at 500 °C for 30 min, evacuated at 500 °C for 20 min, then cooled to room temperature under vacuum. Adsorption of CO was performed at 100 Torr, and corrections for physisorption were made following standard procedures (i.e., initial adsorption followed by evacuation at 1×10^{-6} Torr, and second adsorption).

2.3.2. IR spectroscopy of adsorbed CO

IR spectra of CO adsorbed on selected catalyst samples were obtained using a high-vacuum transmission IR cell, equipped with CaF_2 windows, coupled to a Mattson Cygnus 100 FTIR spectrometer. Powder samples were pressed into a gold wire mesh, which could be resistively heated. Although all reported spectra were obtained using the same instrumental factors, no attempt was made to normalize the absorbance to the weight of catalyst pressed into the wire meshes, which varied slightly from sample to sample. Samples were pretreated by first heating to 350 °C under vacuum for 30 min, cooling to 50 °C and backfilling the cell to 10 Torr H_2, heating again to 350 °C for 10 min, cooling under H_2, evacuating, and finally heating briefly to 350 °C and cooling under vacuum to 50 °C. After recording the background spectrum, CO adsorption was performed by backfilling the cell with CO in a stepwise fashion to 4 Torr. Only the saturation spectra at 4 Torr are reported here.

2.4. XRD

X-ray diffraction (XRD) measurements were performed using Cu Kα radiation and a Scintag X2 diffractometer. Catalyst samples were packed in a cavity, 1 mm deep by 12 mm in diameter, cut into a zero-background quartz plate. Patterns were obtained over the range 10–90°(2θ), focusing on the (311) peak of the fcc lattice (located near 81.2° for Pt). Scintag software was used to fit the peak, and the Debye-Scherrer relation was used to estimate an average diffracting-particle size (taking account of instrumental resolution).

2.5. TEM

Transmission electron microscopy (TEM) was performed with a JEOL 3011 high resolution microscope equipped with an X-ray energy dispersive spectroscopy (EDS) detector. The microscope was operated at 300 kV, with point-to-point resolution of 0.17 nm. Following typical procedures [10], samples were prepared by dispersing a small amount of powder on a 300 mesh carbon-coated copper TEM grid obtained from Structure Probe, Inc.

2.6. NO oxidation

NO oxidation measurements were performed using a 10-channel flow reactor that has been described previously [11]. The feed gas composition was a mixture of 500 ppm NO and 8% O_2 in N_2. The flow rate was 60 standard cm^3/min through each channel. Reactor tubes were loaded with 50 mg of catalyst sample, fixed between quartz wool plugs. Steady state measurements were performed at a series of temperatures from 75 °C to 325 °C, following a 90 min equilibration at each temperature. Measured conversions at each temperature are either reported directly (e.g., figure 7) or converted to overall reaction rates (μmol NO/g_{cat}–s) via a simple model published previously [11] (e.g., figure 8).

3. Results and discussion

CO adsorption capacities are presented in table 2. As expected, the adsorption capacities fall from their initial values with increasing aging temperature for all cata-

Table 2
CO adsorption capacity (at room temperature)

Catalyst name	CO/M after aging at T =				
	(initial)	500 °C	600 °C	750 °C	900 °C
Pt-100-Pd-0	0.668	0.184 0.305[a]	0.041 0.097[a]	0.025	0.007
Pt-90-Pd-10	0.618	0.159	0.070	0.024	0.007
Pt-80-Pd-20	0.473	0.113	0.057	0.024	0.010
Pt-50-Pd-50	0.456	0.182	0.087	0.030	0.014
Pt-0-Pd-100	0.389	0.220	0.185	0.080	0.016

[a]Aged without H_2O.

lysts, but the fractional change between initial and 900 °C is much greater for pure Pt than pure Pd, with the capacity of Pt starting higher and ending lower. The adsorption capacities for intermediate compositions at both of these extremes tend to vary monotonically with Pd content. The difference in initial capacity between Pt and Pd is largely due to different adsorption stoichiometries, approximately 1 CO for each surface Pt atom versus 1–2 surface Pd atoms [12]. The initial average particle size in both cases is thus about the same, ~2 nm. (Note that the presence of water during aging has a pronounced effect on particle coarsening, at least in the case of Pt, where substantially higher adsorption capacities are retained after aging at 500 and 600 °C with no H_2O in the gas mixture.)

IR spectra of CO adsorbed to saturation coverage (at 50 °C) on selected catalysts before aging are shown in figure 1 (at constant relative absorbance but offset for clarity). The spectra from pure Pt and pure Pd catalysts are quite distinct, and agree well in resolution and spectral features to reported data for similarly loaded alumina-supported Pt and Pd catalysts [13–15]. As expected, the spectrum from a physical mixture of equal amounts of these two catalysts closely resembles the superposition of their individual spectra. The spectrum from Pt-50-Pd-50, however, clearly differs from the physical mixture in the range 1850–2000 cm^{-1}, providing evidence that alloy formation has indeed taken place during its synthesis. In particular, the feature near 1970 cm^{-1}, evident in both the pure Pd and 50–50 mixture samples, and usually associated with 2-fold bridging sites on Pd(100) facets [16], is not clearly evident, while enhanced intensity is observed near 1880 cm^{-1} relative to either pure catalyst or the 50–50 mixture.

X-ray diffraction provides further evidence of alloying, though only as particle coarsening progresses, as shown in figure 2. (Before aging, catalysts produced no diffraction features other than those from the alumina support.) The (311) peak position from Pt-50-Pd-50, for example, is approximately half way between that of pure Pt and pure Pd. In general, peaks become sharper and more intense with increasing aging temperature as particles become larger and/or more crystalline. Clearly, the peak from pure Pt at each aging temperature is sharper than that from Pt-50-Pd-50, suggesting that particle

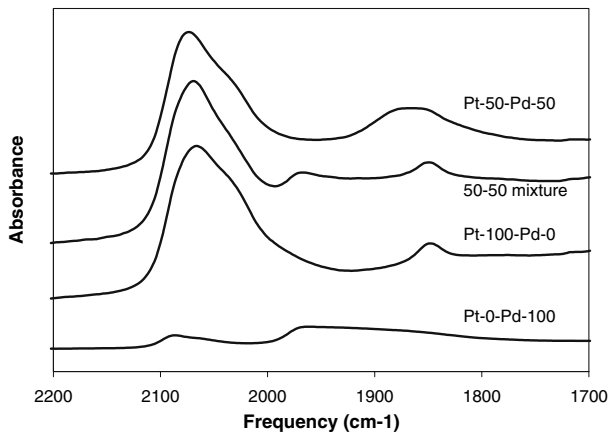

Figure 1. IR spectra of a saturation coverage (at 50 °C) of CO on selected catalysts (before aging) showing effect of alloy formation between Pt and Pd (versus physical mixing).

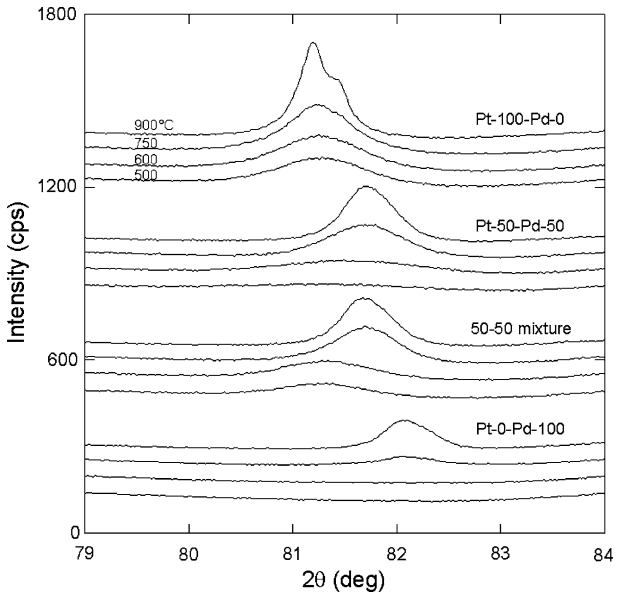

Figure 2. XRD patterns of the (311) peak (fcc lattice) from selected catalysts showing the effects of aging.

coarsening is suppressed in the alloy relative to pure Pt. (The structure in the 900 °C Pt-100-Pd-0 pattern is due to the $K\alpha_1$, α_2 splitting in the X-radiation, which is resolved for sufficiently large diffracting domain size.) In the case of the physical mixture of equal amounts of the pure Pt and Pd catalysts, aging at 500 and 600 °C produces peaks that reflect the pure Pt portion of the sample, whereas aging at 750 and 900 °C produces peaks that are very similar to Pt-50-Pd-50, indicating that alloying takes place *in-situ* [17], starting at some temperature between 600 °C and 750 °C under these particular conditions. Migration of Pt is certainly known to occur very easily under high-temperature lean conditions (via volatile oxide transport), but Pd is apparently more resistant at temperatures somewhat below 750 °C, as shown by the patterns at the bottom of figure 2. The stability of PdO (below 750 °C under 5% O_2) may account for this resistance, which is also reflected in the CO adsorption capacity results (table 2). XRD patterns were taken from several of the aged samples before reduction (1 h at 500 °C under 1% H_2), and in all cases they were found to differ little from those taken after, indicating that (diffracting) particles formed during aging are essentially metallic.

Various XRD parameters derived from the (311) peak of all the catalysts are presented in table 3, and peak positions and normalized intensities (adjusted to correspond to 1wt% Pt equivalent) from the samples aged at 900 °C are plotted in figure 3 along with the expected intensities, varying as $<Z>^2$. The nearly linear dependence of peak position on composition, together with the reasonably good agreement between measured and expected intensities shown in figure 3 provide support for the nominal compositions listed in table 1 and further imply that essentially all of the metal in the samples aged at 900 °C is contributing to the diffraction peak. The smaller intensities observed for each catalyst aged at lower temperatures, as listed in table 3, are thus indicative of a lost contribution from particles that are either too small (less than a few nm) to detect or amorphous. Based on the qualitative observation above, that alloying tends to suppress particle coarsening, the missing intensity might thus produce a bias toward more Pt-rich values in a possible distribution of alloy compositions. This could account for the trend toward Pt peak position in all the alloy catalyst samples as aging temperature decreases. Alternatively, actual alloying could be taking place *in-situ*, as is more obviously the case in the 50–50 physical mixture. The average diffracting-particle size listed in table 3 clearly distinguishes pure Pt from the alloys, but differentiation amongst the various alloy compositions is very slight (apparent at only the lower aging temperatures).

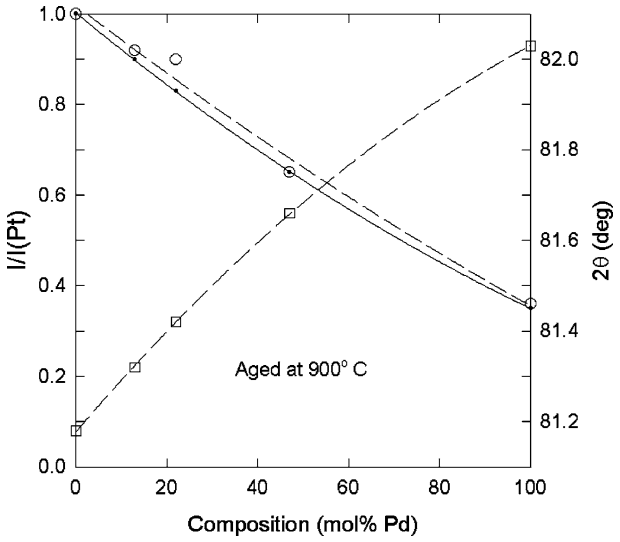

Figure 3. XRD parameters of catalysts aged at 900 °C. The (311) peak position is shown as an open square symbol, the intensity (normalized to Pt at 1wt% equivalent) is shown as an open circle, and the expected intensity ($\propto <Z>^2$) is shown as a small filled circle, through which a solid line is drawn. The dashed lines serve as guides to the eye.

Table 3
XRD parameters – (311) peak

Catalyst name	T (°C)	Position (°)	Intensity (cps)	$<d>$ (nm)
Pt-100-Pd-0	900	81.18	108	43
	750	81.18	100	18
	600	81.19	94	13
	600[a]	81.21	94	12
	500	81.20	79	12
	500[a]	81.22	63	10
Pt-90-Pd-10	900	81.32	99	28
	750	81.32	95	15
	600	81.27	79	9
	500	81.22	70	8
Pt-80-Pd-20	900	81.42	100	28
	750	81.39	91	15
	600	81.41	57	8
	500	81.21	42	6
Pt-50-Pd-50	900	81.66	88	28
	750	81.62	83	15
	600	81.51	70	7
	500	81.34	51	6
50–50 mixture	900	81.63	79	27
	750	81.62	78	18
	600	81.26	61	11
	500	81.22	44	11
Pt-0-Pd-100	900	82.03	46	30
	750	82.01	26	14

[a]Aged without H_2O.

Transmission electron microscopy observations tend to support the XRD inferences about aging-induced variation of particle size with Pd content, as shown by the particle size distributions in figures 4 and 5. (Distributions for Pt-0-Pd-100 are not shown since the contrast was too low to allow definitive discrimination between metal particles and the support.) Statistics derived from the measurements (at least 100 particles

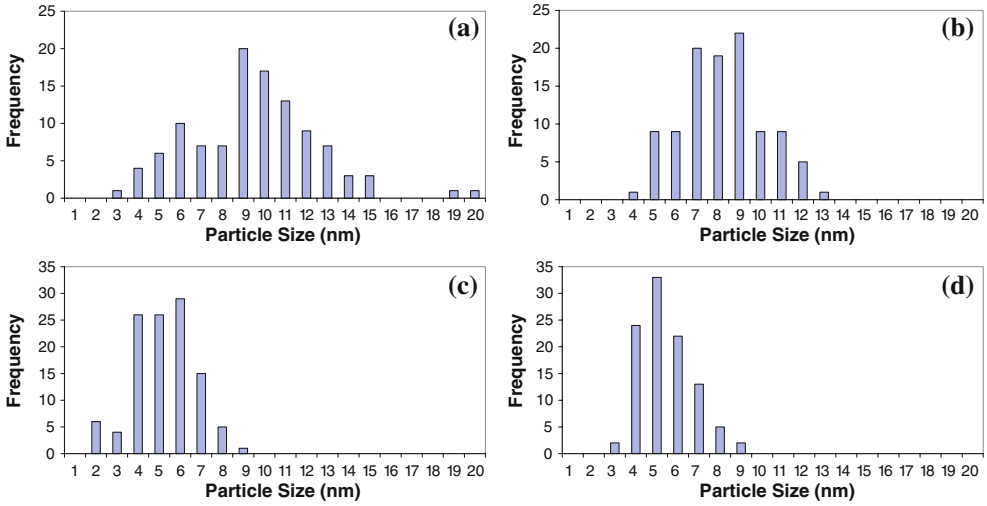

Figure 4. Particle size distributions of catalysts aged at 500 °C, measured by TEM: (a) Pt-100-Pd-0, (b) Pt-90-Pd-10, (c) Pt-80-Pd-20, and (d) Pt-50-Pd-50.

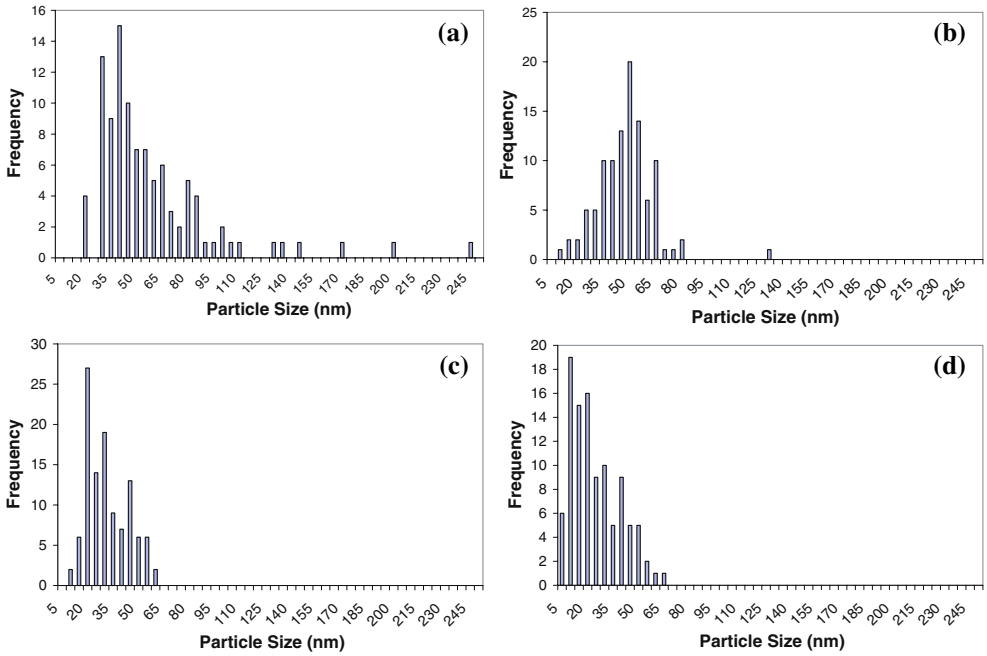

Figure 5. Particle size distributions of catalysts aged at 900 °C, measured by TEM: (a) Pt-100-Pd-0, (b) Pt-90-Pd-10, (c) Pt-80-Pd-20, and (d) Pt-50-Pd-50.

per sample) that produced these distributions are summarized in table 4. Monotonic variations with Pd content clearly become more significant as aging temperature increases, and the anomalously large particles formed at 900 °C in the pure Pt sample are conspicuously absent in samples containing Pd. Typical images obtained from pure Pt samples are shown in figure 6. No particles exceeding 5 nm in size were found in samples of any composition (including pure Pd, according to preliminary experiments using Z-contrast imaging) before aging. Unfortunately, EDS was not able to measure the composition of individual particles in samples before aging, although initial experiments indicate that extended-time (~100 min) EDS mapping could provide the means to check for alloy formation at this stage.

Representative NO oxidation results (measured NO conversion as a function of temperature) are presented in figure 7 for both the set of pure Pt catalysts (before and after aging at the various temperatures) and the corresponding Pt-50-Pd-50 catalysts. The dotted lines are fits to the simple kinetic model described previously (homogeneous, pseudo-first-order NO and effective zero-order O_2, reversible reaction in an isothermal,

Table 4
Particle-size-distribution statistics

Catalyst name	*N*	Mean (nm)	Q1	Min	Med	Max	Q3
500 °C Aging							
Pt-100-Pd-0	109	9.04	6.95	2.80	8.96	19.40	10.90
Pt-90-Pd-10	104	7.69	6.25	3.44	7.70	12.40	8.86
Pt-80-Pd-20	112	4.71	3.76	1.31	4.79	8.75	5.60
Pt-50-Pd-50	101	4.90	3.98	2.61	4.74	8.57	5.52
900 °C Aging							
Pt-100-Pd-0	102	56.25	34.83	15.70	45.25	245.00	65.18
Pt-90-Pd-10	103	45.35	35.55	6.15	45.50	130.00	53.70
Pt-80-Pd-20	111	29.30	18.80	7.61	26.10	59.40	40.00
Pt-50-Pd-50	103	22.09	10.10	2.48	19.00	63.80	31.35

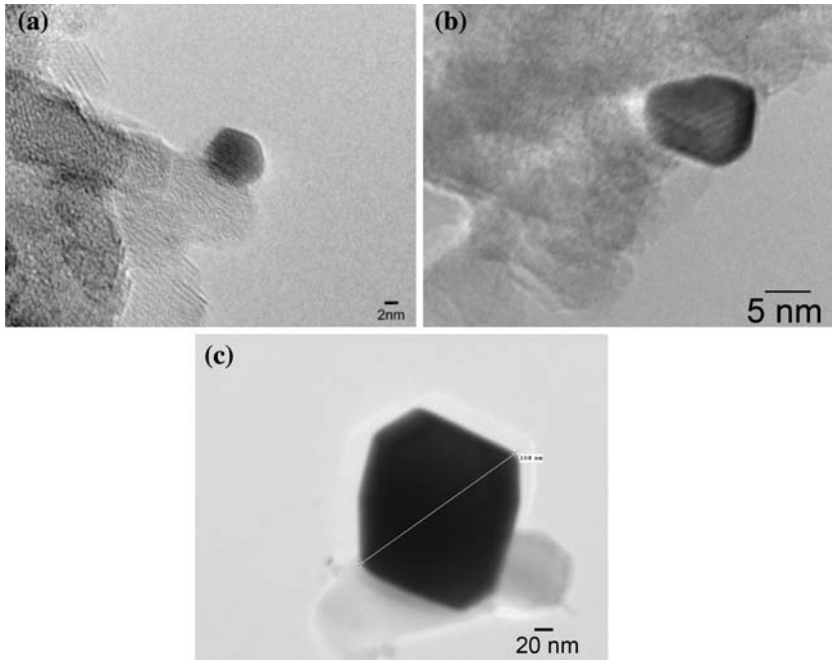

Figure 6. Images of particles from pure Pt samples (a) before aging, (b) aged at 500 °C, and (c) aged at 900 °C. (The particle in (c) is representative of those well out into the tail of the distribution shown in figure 5(a).)

plug-flow reactor [11]). Qualitatively similar data (and fits) were obtained for all of the other samples except the pure Pd catalyst, which exhibits very low NO conversions relative to pure Pt. In particular, the activities of all catalysts initially increase with aging, and then decrease, such that catalysts aged at only 500 °C are generally the most active.

This maximum is also apparent in figure 8, where the reaction rate (at a reaction temperature of 150 °C), is plotted as a function of CO/M for the case of the pure Pt catalysts. Turn-over frequency (TOF; essentially, the rate normalized by CO/M, without any assumptions regarding stoichiometry), also shown in figure 8 for all the catalysts except pure Pd, appears to be fairly independent of composition over the range examined and increases monotonically as the CO/M values decrease to the lowest values measured in this study. The rate maximum observed for pure Pt (occurring at CO/M between approximately 0.1–0.2) thus reflects the competing effects of decreasing CO/M and increasing TOF with aging severity. The average Pt particle size at this point is in the range 5–10 nm.

The 50–50 physical mixture provides an interesting comparative case. Although its NO oxidation behavior follows the same qualitative pattern, it does not achieve the same maximum rate as the Pt-50-Pd-50 catalyst since it performs like a pure Pt catalyst with only half the loading (and thus half the rate) at the stage where NO conversion peaks (after aging at ~500 °C). Moreover, as shown in table 3, the metal particle size is 11 nm at 500–600 °C – already slightly beyond the optimal range of 5–10 nm. In contrast, the Pt-50-Pd-50 sample shows clear evidence of alloy formation by 500 °C (figure 2) and an XRD diameter of 6 nm. Alloying finally occurs in the

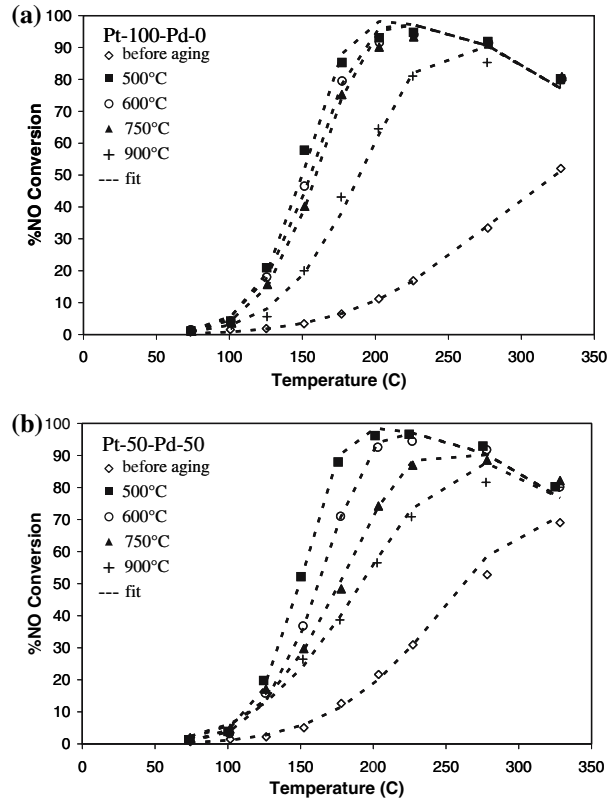

Figure 7. NO conversion (to NO_2) as a function of temperature over (a) Pt-100-Pd-0 and (b) Pt-50-Pd-50, before and after aging at the indicated temperatures. Dotted lines are fits to the kinetic model described in Ref. [11].

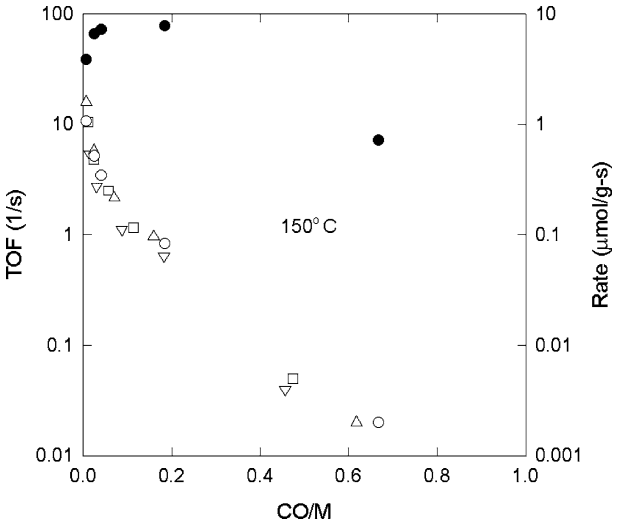

Figure 8. NO oxidation rate to NO_2 (μmol NO/g_{cat}–s) at 150 °C over Pt-100-Pd-0 as a function of CO/M (solid circles) and turn-over frequency (TOF) at 150 °C as a function of CO/M for Pt-100-Pd-0 (open circles), Pt-90-Pd-10 (open up triangles), Pt-80-Pd-20 (open squares), and Pt-50-Pd-50 (open down triangles).

50–50 physical mixture after aging at higher temperatures (figure 2), yielding particles of comparable size to the Pt-50-Pd-50 catalyst (table 3), but the NO conversion rate has fallen well below the maximum at this stage. While *in situ* alloy formation, characteristic of the physical mixture, still has benefits relative to pure Pt under high-temperature aging conditions, the results of this study show that synthesis techniques that produce alloy particles from the start offer a significant performance advantage for applications where exposure to oxygen-rich exhaust gases can be controlled to temperatures between roughly 600 °C and 750 °C.

The increase in turn-over frequency for NO oxidation with decreasing dispersion (or CO/M) has been observed previously [e.g., 18], and a variety of explanations involving, for example, Pt oxidation [19] or facet-dependent specific activities may apply. Another possibility, motivated by recent mechanistic studies identifying gas phase NO_2 inhibition [19], is that stored NO_x species – stable on alumina at monolayer coverages up to temperatures of at least 350 °C [20] – may inhibit the NO oxidation activity of small metal particles more than large ones. If so, catalysts made from support materials that store less NO_x than alumina (or hold it more weakly) might be expected to perform better in NO oxidation. The previous NO oxidation study from our laboratory [11], for example, showed substantially higher TOFs for silica- versus alumina-supported Pt catalysts. Regardless of the explanation for the increase in TOF with decreasing CO/M, the similarity in the kinetics between pure Pt and the alloy samples, including the quality of the model fits, similarity of rate constants and apparent activation energies, and the nearly equal TOFs for a given CO/M, suggests that alloying Pd with Pt does not fundamentally change the mechanism of the surface-catalyzed NO oxidation.

Finally, it is interesting to consider possible explanations for the effects of Pd on alloy-particle coarsening and NO oxidation activity. One explanation of the coarsening effect, proposed in an earlier study that included detailed analysis of particle structure, is that Pd forms a shell around a Pt (or Pt-rich) core, effectively blocking Pt from access to the gas phase, and thus blocking vapor phase transport of Pt via volatile oxides [6]. This situation seems unlikely in the present case, since the catalytic behavior of Pd for NO oxidation is so different from that of Pt. Instead, it may be that only a small concentration of Pd on the surface of the particles is required in order to disrupt the process (possibly involving several steps) that eventually leads to the formation and volatilization of Pt as PtO_2. If so, the surface could remain essentially Pt-like, thus accounting for the retention of NO oxidation activity akin to Pt rather than Pd.

4. Summary

Alloying Pt with Pd in alumina-supported catalysts for NO oxidation was found to produce the desired

effect – suppression of particle coarsening upon aging under lean conditions – and hence, more effective utilization of the noble metals. Further, the turn-over frequency for NO oxidation was found to be relatively insensitive to a Pd content approaching 50 mol%. These, together with the observation of a broad maximum in NO oxidation rate as a function of dispersion, point to the value of targeting an optimum particle size, stabilized through alloy formation with as much Pd as possible (at least 10 mol%), in order to minimize the amount of Pt that is required for NO oxidation in lean-combustion exhaust-gas after-treatment applications (assuming, of course, that Pt continues to be much more expensive than Pd). Rather than shifting the mean particle size, the main effect of Pd alloying is to prevent the formation of a small number-fraction of extremely large particles (greater than ~100 nm) observed for pure Pt after high-temperature aging in oxygen-rich gas mixtures. Although the reason for this is not known, the results of the present study suggest that alloying introduces small concentrations of Pd in the surface region of the Pt–Pd alloy particles, thereby mitigating the formation of volatile Pt oxides without significantly changing the Pt-like nature of the surface for NO oxidation.

Acknowledgments

The authors gratefully acknowledge the support of C. T. Goralski, Jr. during the early stages of this work, useful discussions with P. J. Schmitz, A. R. Drews, and S. J. Harris on the subject of NO oxidation, and technical assistance from J. Hangas. The JEOL 3011 TEM resides at EMAL, a facility of the University of Michigan, which is funded in part under NSF Grant DMR-9871177.

References

[1] N. Takahashi, H. Shinjoh, T. Iijima, T. Suzuki, K. Yamazaki, K. Yokota, H. Suzuki, S. Miyoshi, S. Matsumoto, T. Tanizawa, T. Tanaka, S. Tateishi and K. Kasahara, Catal. Today 27 (1996) 63.
[2] M. Li, J. Henao, Y. Yeom, E. Weitz and W.M.H. Sachtler, Catal. Lett. 98 (2004) 5.
[3] P. Hawker, N. Myers, G. Huthwohl, H.T. Vogel, B. Bates, L. Magnusson and P. Bronnenberg, *Society of Automotive Engineers*, Paper No. 970182, 1997.
[4] G.W. Graham, H.-W. Jen, W. Chun, H.P. Sun, X.Q. Pan and R.W. McCabe, Catal. Lett. 93 (2004) 129.
[5] M. Chen and L.D. Schmidt, J. Catal. 56 (1979) 198.
[6] A. Morlang, U. Neuhausen, K.V. Klementiev, F.-W. Schutze, G. Miehe, H. Fuess and E.S. Lox, Appl. Catal. B 60 (2005) 195.
[7] R.J. Kudla, H.-W. Jen, P.J. Schmitz, C.T. Goralski Jr., R.W. McCabe and G.W. Graham, 19th NACS (2005).
[8] A. Renouprez, A. Malhomme, J. Massardier, M. Cattenot and G. Bergeret, Stud. Surf. Sci. Catal. 130C (2000) 2579.
[9] F. Morfin, J.-C. Sabroux and A. Renouprez, Appl. Catal. B 47 (2004) 47.
[10] L. Wei and T. Li, Micros. Res. Tech. 36(5) (1997) 380.
[11] P.J. Schmitz, R.J. Kudla, A.R. Drews, A.E. Chen, C.K. Lowe-Ma, R.W. McCabe, W.F. Schneider and C.T. Goralski Jr., Appl. Catal. B 67 (2006) 246.
[12] R.L. Moss, in: *Experimental Methods in Catalytic Research*, eds. R.B. Anderson and P. T. Dawson (Academic Press, New York, 1976) p. 74.
[13] A. Bourane, S. Derrouiche and D. Bianchi, J. Catal. 228 (2004) 228.
[14] M. Skotak, Z. Karpinski, W. Juszczyk, J. Pielaszek, L. Kepinski, D.V. Kazachkin, V.I. Kovalchuk and J.L. d'Itri, J. Catal. 227 (2004) 11.
[15] M. Benkhaled, S. Morin, Ch. Pichon, C. Thomazeau, C. Verdon and D. Uzio, Appl. Catal. A 312 (2006) 1.
[16] X. Xu and D.W. Goodman, J. Phys. Chem. 97 (1993) 7711.
[17] G.W. Graham, H. Sun, H.-W. Jen, X.Q. Pan and R.W. McCabe, Catal. Lett. 81 (2002) 1.
[18] J.-H. Lee and H.H. Kung, Catal. Lett. 51 (1998) 1.
[19] S.S. Mulla, N. Chen, L. Cumaranatunge, G.E. Blau, D.Y. Zemlyanov, W.N. Delgass, W.S. Epling and F.H. Ribeiro, J. Catal. 241 (2006) 389.
[20] H.-W. Jen (unpublished data).